Chemical Engineering Journal 430 (2022) 132760

Contents lists available at ScienceDirect

Chemical Engineering Journal

journal homepage: www.elsevier.com/locate/cej

Reaction rate enhancement by reducing surface diffusion barriers of guest molecules over ZSM-5 zeolites: a structured illumination microscopy study

Shichao Peng [a,c], Hua Li [a,*], Wenjuan Liu [b,c], Junyi Yu [a,c], Zhaochao Xu [b], Mao Ye [a,*], Zhongmin Liu [a,c]

[a] National Engineering Laboratory for Methanol-to-Olefins, Dalian National Laboratory for Clean Energy, Dalian Institute of Chemical Physics, Chinese Academy of Sciences, Dalian 116023, China
[b] Key Laboratory of Separation Science for Analytical Chemistry, Dalian Institute of Chemical Physics, Chinese Academy of Sciences, Dalian 116023, China
[c] University of Chinese Academy of Sciences, Beijing 10049, China

ARTICLE INFO

Keywords:
Zeolite catalysis
Surface barriers
Catalytic reaction rate
ZSM-5
Structured illumination microscopy

ABSTRACT

Mass transfer of guest molecules is crucial for zeolite catalysis. Compared to intracrystalline diffusion, the surface barriers in zeolite catalysis have been less understood. Taking furfuryl alcohol oligomerization catalyzed by ZSM-5 zeolites as model reaction, here we present a single-crystal level study and gain insight into the surface barriers induced spatiotemporal evolution of oligomer products using structured illumination microscopy (SIM). It is shown that, as a result of the enhanced accessibility to zeolite crystals, promoting the surface permeability leads to the increase in catalytic reaction rate that is characterized as the generation rate of oligomer products.

1. Introduction

Zeolites have been widely used as solid acid catalysts in a variety of important industrial processes such as fluid catalytic cracking (FCC),[1] methanol-to-olefins[2] and isomerization of aromatics,[3] owing to the unique shape selectivity.[4] However, the catalytic performance of zeolites is meantime plagued by the diffusion limitations of guest molecules, which would lead to the fluctuations of apparent catalytic activity.[5,6] Controlling the diffusion of guest molecules has long been a big challenge in the rational design of zeolites and the corresponding zeolite-catalyzed reactions, calling for deeper understanding of the diffusion mechanism in zeolite catalysis.

Recent studies found that, in addition to intracrystalline diffusion defined as the molecular transport into the intracrystlline pore network that is inherent to the topological structure of nanoporous materials, surface permeability represents another significant mass transfer mechanism associated with the molecular permeation through the external surface.[7–9] The origin of surface barriers is very complicated, and among many others, pore blockage, for example, has been considered as one of the important causes of surface barriers in the presence of imperfect crystal surfaces.[10–14] Previous researches have revealed that surface barriers can even dominate the mass transfer resistance in zeolites,[15–18] showing great potential in modulating zeolite catalysis. But in practical processes the molecular diffusion is always closely coupled with the reaction, directly unveiling the influence of the diffusion of guest molecules in catalytic reaction remains an extremely hard, if not impossible, task.

Very recently there are increasing interests in revealing the role of surface resistance in catalytic processes.[19–21] Rao *et al.* showed that incorporating the surface barriers could make their diffusion model a good fit with the experimental data for ZSM-5 zeolites in benzene alkylation with ethylene reaction, which otherwise shows a substantiable deviation.[19] In a previous work, we demonstrated that the catalytic lifetime and products selectivity in methanol-to-olefins (MTO) reaction can be modulated by controlling the surface permeability via surface modification of SAPO-34 zeolites.[20] Hu *et al.* also showed that the surface barriers can affect the conversion of the isomerization of n-pentane by depositing SiO_2 on the surfaces of Pt/Beta.[21] These studies, however, almost remain at the macroscopic cognition. The absence of detailed information on the interplay between surface barriers and catalytic reaction at single-crystal level still hinders further understanding and thus quantifying the mass transfer in zeolite catalysis.

In this work, we intend to demonstrate the significant effect of surface barriers on the catalytic reaction at single-crystal level by considering the oligomerization of furfuryl alcohol (FA) catalyzed by ZSM-5

* Corresponding authors.
E-mail addresses: lihua@dicp.ac.cn (H. Li), maoye@dicp.ac.cn (M. Ye).

https://doi.org/10.1016/j.cej.2021.132760
Received 11 July 2021; Received in revised form 10 September 2021; Accepted 28 September 2021
Available online 2 October 2021

zeolites as model reaction.[22–24] In doing so, we quantitatively modulated the surface permeability of the ZSM-5 zeolites, and then evaluated the induced change in catalytic reaction rate based on the generation rate of the oligomer products. Essentially, the structured illumination microscopy (SIM) was used to illustrate the spatiotemporal evolution of the oligomer products at single-crystal level during the reaction.

2. Material and methods

2.1. Synthesis and modification

ZSM-5 zeolites were hydrothermally synthesized following Sang *et al.*[25] In the synthesis, water glass, aluminum sulfate and n-Butylamine were utilized as Si source, Al source and organic directing agents, respectively. Concentrated sulfuric acid was applied to neutralize the excess sodium oxide. First, $Al_2(SO_4)_3{\cdot}18H_2O$ was dissolved into a part of distilled water to get a solution A, followed by the addition of concentrated H_2SO_4, and water–glass and the other part of distilled water were mixed together to form solution B. Then, solution A was dropwise added to solution B under stirring to obtain a homogenous gel with the composition of 1.0 SiO_2: 0.01 Al_2O_3: 0.08 Na_2O: 0.2 BTA: 40 H_2O. Finally, the gel was transferred to a stainless-steel autoclave and heated at 175 °C for 48 h. The products were collected by filtration, washed with deionized water, and dried at 100 °C in air for 12 h. The synthesized ZSM-5 zeolites were denoted as ZSM-5-P.

For the surface modification, 1.0 g of ZSM-5-P zeolites was added to 50.0 mL hydrochloric (HCl) solution. After magnetic stirring the mixture at 80 °C for 2 h, the slurry was filtered, washed by distilled water for three times until pH = 7, and dried at 120 °C in air for 12 h. The post-treated zeolites were denoted as ZSM-5-H. All samples were calcined at 650 °C for 12 h to remove the organic template and ion-exchanged three times with 1.0 mol/L NH_4NO_3 followed by calcination at 550 °C for 4 h.

2.2. Characterizations

X-ray diffraction (XRD) patterns were recorded using a PANalytical X'Pert PRO X-ray diffractometer with Cu-Kα radiation (λ = 0.15418 nm) in the 2θ range from 5 to 40°. Elemental analyses were examined by a Philips Magix-601 X-ray fluorescence (XRF) spectrometer and Horiba X-max energy dispersive X-ray (DEX) spectrometer. Helium ion microscopy (HIM) images were recorded by using a Zeiss ORION Nanofab helium ion microscope. Hydrophilicity of the sample was detected by Kruss DSA100 contact angle meter. Nitrogen adsorption–desorption isotherms were measured at −196 °C on a Micromeritics ASAP2020. The samples were outgassed at 350 °C for 6 h prior to the sorption measurements. The total pore volume is determined from the adsorbed volume at p/p_0 = 0.99. Based on the Brunauer-Emmett-Teller (BET) methods, the total BET surface area can be calculated. The micropore and mesopore size distributions were analyzed by the NLDFT method and BJH algorithm, respectively. Temperature-programmed desorption (TPD) of ammonia were performed on a Micrometric 2920 chemisorption analyzer. During the experiments, 100 mg the sample of 40–60 mesh was loaded into a quartz U-shaped reactor and pretreated at 600 °C for 1 h in flowing He, and then cooled down to 100 °C and saturated with $NH_3{\cdot}NH_3$-TPD was carried out from 100 to 600 °C at a constant heating rate of 10 °C * min^{-1}. Thermogravimetric analysis (TGA) analysis was performed on a TA SDTQ600 analyzer with a temperature-programmed rate of 10 °C * min^{-1} under flowing air (100 mL * min^{-1}) from room temperature to 900 °C.

Diffuse reflectance infrared Fourier transform spectroscopy (DRIFTS) were conducted on a Bruker Vextex70 spectroscope equipped with an MCT detector at resolution of 4 cm^{-1} and 16 scans under flowing N_2. UV/Vis diffuse reflectance spectra (DRS) were performed with a PerkinElmer Lambda950 using a UV–Vis-NIR spectrophotometer. Prior to the measurement, the zeolite samples were pressed into the diffuse reflectance infrared chamber with a ZnSe window and heated at 350 °C to remove the adsorbed water for DRIFTS while kept at room temperature for UV/Vis-DRS. In each experiment, the quantities of sample were kept the same.

The uptakes of ethylcyclopentane (ECP, Aladdin, greater than 99.0 %) on the ZSM-5 zeolites were carried out by intelligent gravimetric analyzer (IGA) equipped with a mesh type sample cell. The ZSM-5 catalyst (30.0 mg) was added to the chamber and evacuated at 450 °C for 4 h. The increase in mass with the adsorption of ECP over ZSM-5 zeolites were measured at 25 °C (0 → 1 and 1 → 2 mbar).

The structure illumination microscopy (SIM) studies were performed with a Nikon N-SIM with a × 100/NA 1.49 oil immersion TIRF objective lens (CFI HP). The super-resolution microscopy system contains a motorized inverted microscopy ECLIPSE Ti2-E and ORCA-Flash 4.0 sCMOS camera (Hamamatsu Photonics K.K.). There are four channels with corresponding excitation wavelength in SIM, i.e. $\lambda = 405$ (detection at 435–485 nm), 488 (detection at 500–545 nm), 561 (detection at 570–640 nm) and 640 nm (detection at 663–738 nm). All images are focused at the center of the crystal.

2.3. Quantification of diffusion

The uptake curves of ethylcyclopentane (ECP) measured by IGA were fitted with the improved dual resistance model (DRM) to obtain the surface permeability (α) and intracrystalline diffusivity (D) following Gao *et al.*[26] Prior to D, the surface permeability α can be decoupled from apparent diffusion by a concise quadratic expression, which is derived from Fick's law by applying the Laplace transform and Taylor's expansion, shown as

$$\frac{m_t}{m_\infty}\Big|^{\sqrt{t}\to 0} \cong \frac{\alpha}{l}(\sqrt{t})^2 \tag{1}$$

where m_t/m_∞ is the normalized loading, t the uptake time, and l the equivalent radius, respectively. The simplified equation can be applied to obtain α by the initial uptake data. Subsequently, with the information of surface barriers, it can be straightforward to gain the intracrystalline diffusivity by fitting the whole uptake curves with DRM according to

$$\frac{m_t}{m_\infty} = 1 - \sum_{n=1}^{\infty} \frac{2L^2 \exp\left(-\frac{\beta_n^2 D t}{l^2}\right)}{(\beta_n^2 + L^2 + L)\beta_n^2}; \beta_n \tan\beta_n = L = \frac{\alpha l}{D} \tag{2}$$

As DRM is derived according to the plane sheet, the equivalent radius should be redefined based on the shape of nanoporous crystalline materials. In this work, ZSM-5 zeolites were adopted, which is an approximate cuboid. Herein, the equivalent radius can be defined as $l = \sqrt[3]{abc}/4.06$, where *a,b* and *c* represent the length, width and height of crystal, respectively. According to this approach, the uptake curves of ECP can be fitted to quantify the surface barriers and intracrystalline diffusivity.

2.4. Fluorescence experiment

In the reaction experiment, furfuryl alcohol olimerization was utilized as a fluorogenic reaction model. 10 mg of zeolite samples were added to 1.0 mL of water-furfuryl alcohol mixture (furfuryl alcohol content 1.0 % vol) and left to react under oscillation at room temperature. For microscopic imaging, a few stained zeolite samples were taken out from the slurry and fast washed by distilled water for three times, then placed in a liquid cell for measurement. Here, the exited laser of 561 nm (detection at 570–640 nm) was chosen for determined the spatial location of furfuryl alcohol olimerization within the zeolite crystal. Then, the rest of slurry was filtered washed by anhydrous ethanol for three times, and evaporated at room temperature for UV/

Vis-DRS record.

3. Results and discussions

3.1. Quantitative control of surface barriers over ZSM-5 zeolites

In order to obtain the zeolites with different surface barriers, surface modification methods need to be developed. Etching is an efficient method to eliminate surface resistance.[27,28] Conventionally, the zeolites were post-treated with hydrofluoric acid to remove the surface defect, thereby increasing the diffusion.[27] However, this would also damage the internal structure and thus the acid sites.[28] Here, we carefully adjust the strength of acid etching to remove the surface imperfections and meanwhile maintain the structure, texture and acid property. First, ZSM-5 zeolites were hydrothermally synthesized[25] and named as ZSM-5-P. Then, parts of ZSM-5-P samples were moderately etched by hydrochloric acid to reduce surface barriers, and donated as ZSM-5-H. As organic template could effectively prevent hydrochloric acid inside the zeolites, the internal structure of crystals could be almost fully preserved. Furthermore, the decrease of acid strength in etching can assure the stability of zeolites, and thus the destruction of crystals can be avoided.

Fig. 1 shows both the external morphology and internal structure of the ZSM-5-P and ZSM-5-H. As can be seen from helium ion microscopic (HIM) imaging (Fig. 1a and 1b), the crystal size of ZSM-5 zeolites is about 20 × 10 × 10 μm^3, and the crystal morphology only slightly changed after modification. Before modification, there is a layer of amorphous-alike phase on ZSM-5-P crystal surface (Fig. 1a), and the sedimentary could be washed down by hydrochloric acid in ZSM-5-H (Fig. 1b). In order to explore the internal structure of the crystal, partial removal of template was adopted to obtain the structural information inside the samples through structured illumination microscopy (SIM).[29] In Fig. 1c and 1d, hourglass patterns can be recognized, which is indicative of 90° intergrowths characteristic for ZSM-5 crystal, illustrating that the internal grain boundaries are intact after treatment.[12,29] Besides, template-removal experiment by thermal gravimetric analyzer (TGA) illustrates almost no difference in template content between two samples (Figure S1), which further indicates that the internal structure can be preserved after etching.

To further confirm the changes by etching, the texture, pore structure and acid properties of ZSM-5 zeolites were investigated. The XRD patterns (Fig. 2a) manifest the characteristic diffraction peaks of the typical MFI-type structure. Compared to ZSM-5-P, the relative crystallinity of ZSM-5-H, calculated based on the sum of the peak intensities in the 22° < 2θ < 25°,[30,31] is almost invariant (Table S1). The pore size distribution and pore structure parameters can be obtained by the N_2 adsorption–desorption isotherm (Fig. 2b). Both samples have similar total pore volume, specific surface area (Table S1) and micropore distribution (Fig. 2c). However, there are some differences in the mesopores distribution (Fig. 2d) and external surface area (Table S1). ZSM-5-P contains parts of mesopores and external surface area, indicating the existence of amorphous-alike phase on the crystal surface. These are both reduced in ZSM-5-H, showing the removal of the surface layer by etching. The Si/Al ratios of the bulk phase and the crystal edge are also summarized in Table S1, which both increase after acid etching, indicating the amorphous-alike phase would be Al-rich. The NH_3-TPD curves (Fig. 2e) display two separated peaks referring to weak and strong acid, corresponding to 226 and 415 °C. There is no significant change in acid strength and density after etching except for a little decrease in weak acid density (Table S1). From DRIFT spectra (Fig. 2f), the absorption bands at around 3602 cm^{-1} are contributed to bridging hydroxyl referring to Brønsted acid sites, which are nearly uniform in both samples. The external surface acidity can be investigated by SIM images of uncalcined pyridine-adsorbed zeolites (Figure S2).[32] Compared with ZSM-5-P, an improvement of fluorescence intensity (Figure S2c) in ZSM-5-H indicates a slight increase in the external surface acidity, probably due to the removal of the amorphous-like phase leading to the exposure of concealed acid sites.

The uptake curves of guest molecules (Figure S4) were measured by intelligent gravimetric analyzer (IGA), and surface permeability (α) and intracrystalline diffusivity (D) can be quantified following our previous work.[26] In the furfuryl alcohol (FA) oligomerization experiment, FA is taken as the probe, and oligomerization will occur in ZSM-5 with Brønsted acid under room temperature. Therefore, in order to avoid the influence of reaction on the diffusion measurement, ethylcyclopentane (ECP), rather than FA, was used as the probe molecule for deriving α and D. Although ECP and FA have different physical and chemical properties such as polarity and reactivity, it is reasonable to use an inert probe with the similar size and structure instead of the active reactant to characterize the change of α and D after surface modification.[20] Fig. 3 shows α and D of ECP under different pressures at 25 °C. It can be seen that the two samples have almost unchanged diffusivity D, which is consistent with the similar intracrystalline characteristics of these two samples. But an increase of 30 % in α can be observed for ZSM-5-H compared to that for ZSM-5-P, indicating a reduction of surface barriers by etching.

From the characterizations mentioned above, we speculate that the surface barriers of guest molecules might be resulted from the Al-rich amorphous-alike phase with mesopores on the external surface of zeolites, which would block the pore mouth and prevent guest molecules from entering crystals. By using moderate acid etching we could effectively remove the redundant sediment, open the orifices and thus facilitate mass transfer on the crystal surface.

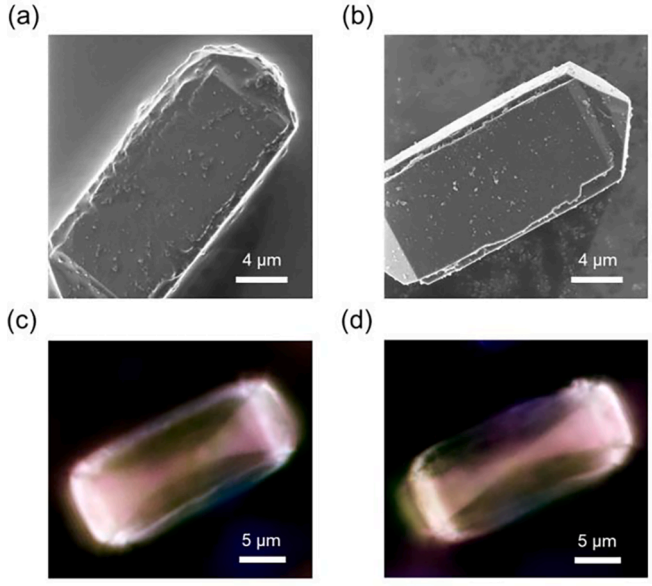

Fig. 1. HIM images of ZSM-5-P (a) and ZSM-5-H (b), SIM microphotographs of ZSM-5-P (c) and ZSM-5-H (d) by partial-removal template in 500 °C for 30 min.

3.2. Effect of surface barriers on catalytic reaction rate

Furfuryl alcohol oligomerization experiments were then carried out to evaluate the ZSM-5 samples at room temperature, and the stained zeolites with different reaction times were measured by UV/Vis diffuse reflectance spectroscopy (UV/Vis-DRS) instrument. Furfuryl alcohol undergoes oligomerization reaction with the acid catalysis of ZSM-5 zeolites. As shown in Fig. 4a-d, there are obvious absorption peaks at the wavelength of 465, 560, 590, 660 and 745 nm, respectively. The absorbance represents the quantity of catalytic products. Compared with the pristine ZSM-5-P, the modified ZSM-5-H has stronger absorptions at different reaction time as shown in Fig. 4a-d, indicating higher catalytic reaction rate. Considering that there is no obvious change in the internal

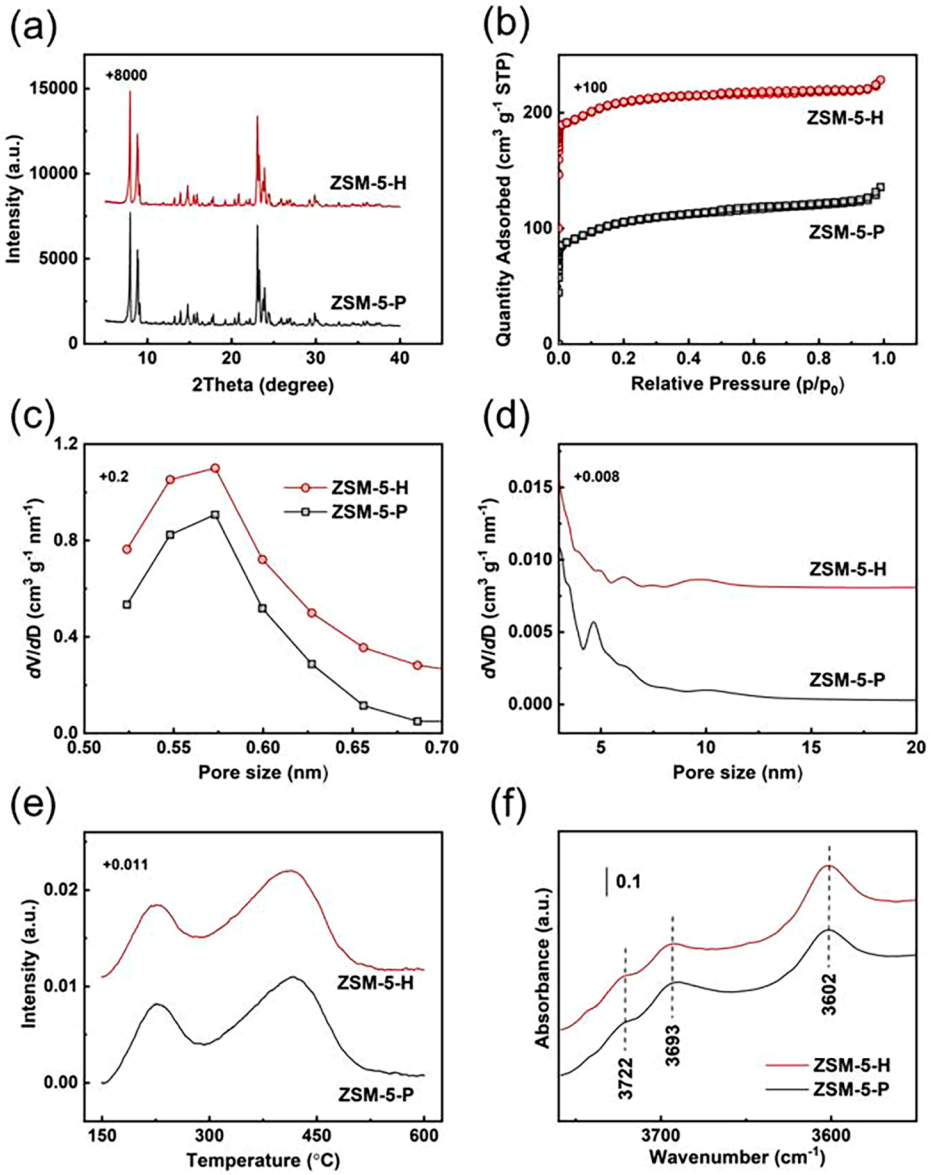

Fig. 2. (a) XRD patterns. (b) N_2 adsorption–desorption isotherms. (c) The micropore size distribution analyzed by NLDFT method. (d) The mesopore size distribution calculated by BJH algorithm. (e) NH_3-TPD profiles. (f) DRIFT spectra.

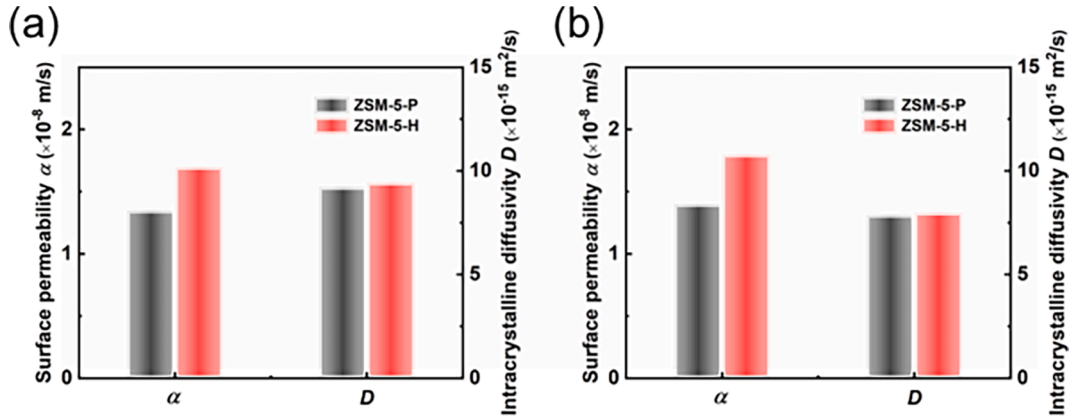

Fig. 3. Surface permeability (α) and intracrystalline diffusivity (D) of ethylcyclopentane at 25 °C in two ZSM-5 samples derived by the uptake rates (Supporting Information) under 0 → 1 mbar (a) and 1 → 2 mbar (b).

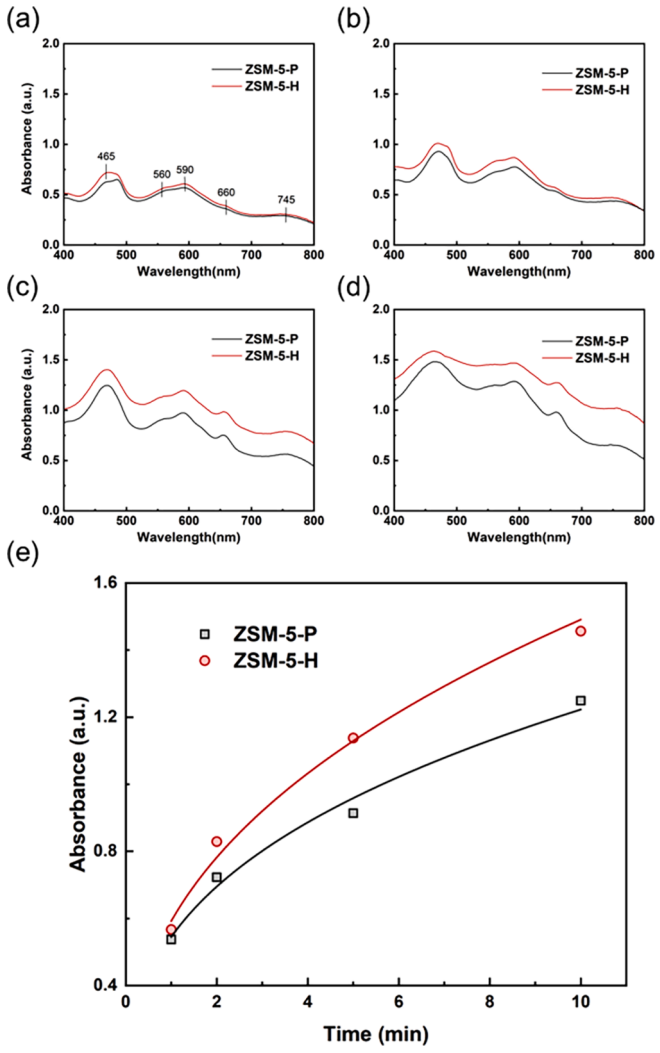

Fig. 4. UV/Vis-DRS profiles of the condensation of furfuryl alcohol catalyzed in the samples of ZSM-5-P and ZSM-5-H with reaction time at (a) 1 min, (b) 2 min, (c) 5 min and (d) 10 min. (e) The absorbance at the wavelength of 560 nm with different reaction time in two samples. The scatters represent the experimental data while solid lines are fitting results. The absorbance is fitted as $A_P = 0.545t^{0.351}$ for ZSM-5-P and $A_H = 0.592t^{0.401}$ for ZSM-5-H. The correlation coefficient R^2 of all fitting is greater than 0.99.

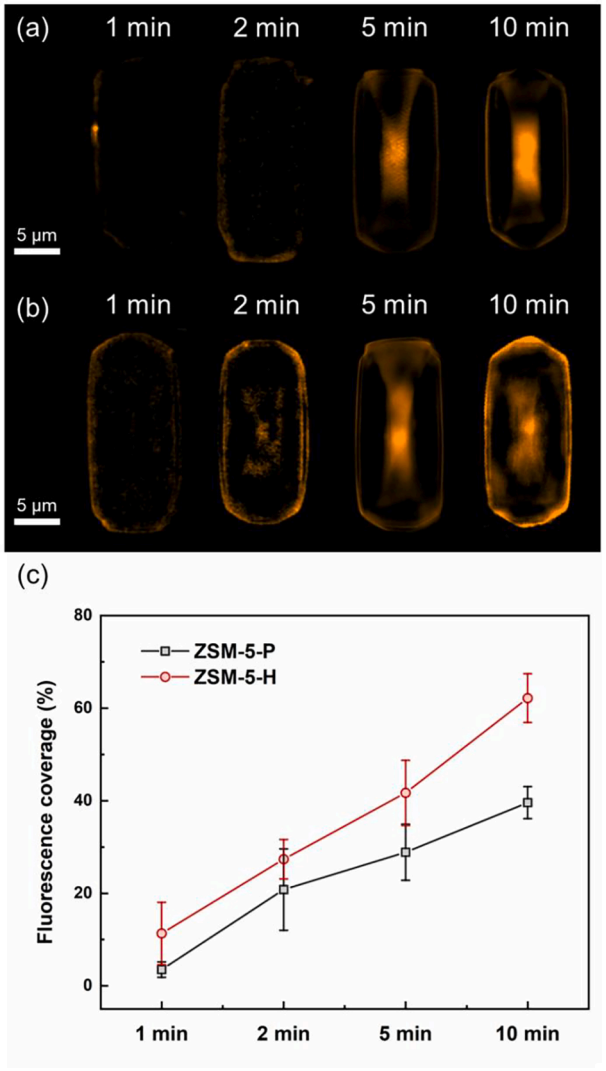

Fig. 5. SIM imaging of the condensation of furfuryl alcohol catalyzed in typical zeolite crystals of ZSM-5-P (a) and ZSM-5-H (b) with different reaction time (561 nm lasers, detection at 570–640 nm, false colors) and corresponding average fluorescence coverage of multiple crystals (c).

structure and acid properties, we anticipate that these phenomena are mainly caused by the decrease in surface barriers. That is, the samples with higher surface permeability exhibit better catalytic ability. In order to quantify the influence of surface barriers on the catalytic reaction, the peak at the wavelength of 560 nm was selected to represent the typical oligomer products[23,24] as shown in Fig. 4e. By assuming that the absorbance at the wavelength of 560 nm, A, is proportional to the concentration of oligomer products (C), we can estimate the oligomerization rate of furfuryl alcohol r by $r = \frac{dC}{dt} \frac{dA}{dt}$. From Fig. 4e, the mean oligomerization rate of furfuryl alcohol for ZSM-5-H is 25 % higher than that for ZSM-5-P. This indicates that an improvement in surface permeability results in an increase in apparent catalytic reaction rate.

In order to further explore how surface barriers affect the catalytic reaction rate at single-crystal level, structured illumination microscopy (SIM) was utilized to obtain the spatiotemporal images of the furfuryl alcohol oligomers over ZSM-5 crystals. The fluorescence imaging techniques can realize the tracking of the positions of catalytic reactions in an individual crystal by detecting the presence of fluorescent molecules, [22–24] which can intuitively visualize how the catalytic reaction evolves at the single zeolite crystal level. Fig. 5a and 5b display the fluorescence imaging of ZSM-5-P and ZSM-5-H, respectively. It is shown that at the initial stage, as furfuryl alcohol primarily contacts the edge of the crystal and oligomers, the generation of fluorescent signal starts from the outer rim. With the reaction proceeding, the fluorescence gradually appears at the center of crystal and forms an hourglass pattern, which may be caused by the internal barriers resulted from the internal grain boundaries.

Compared with ZSM-5-P, the ZSM-5-H exhibits the rapid fluorescence migration inside the single crystal. Specifically, during the initial stage (at reaction time of 1 min), at almost all edges of the ZSM-5-H crystal the fluorescence signals are quickly generated. As reaction proceeds (at reaction time of 2 min), in the ZSM-5-H crystal the fluorescent signal appears preferentially in the center. However, even at reaction time of 2 min, the fluorescent signal inside ZSM-5-P crystal is still quite weak. After 5 min, fluorescent products gradually fill the crystal in both samples. To quantify the effect of surface barriers on the spatiotemporal evolution of the oligomer products, we recorded the fluorescence coverage of both zeolite crystals, as shown in Fig. 5c. It can be seen that the etched ZSM-5-H zeolite crystals are more rapidly covered by fluorescence products, indicating an increase in the utilization efficiency of zeolite crystals. These observations demonstrate that the increase of

surface permeability can promote the accessibility of the zeolites, enhance the catalytic reaction in the interior of the crystals, and thus improve the catalytic reaction rate.

4. Conclusions

In this work, we present a single-crystal level study on how the surface barriers affect the catalytic reaction in the ZSM-5 zeolites by use of structured illumination microscopy. Through improved surface etching, the surface permeability of the guest molecules over ZSM-5 can be enhanced without changing the intracrystalline properties. The furfuryl alcohol oligomerization experiments demonstrate that an improvement in surface permeability leads to the increase in catalytic reaction rate. The spatiotemporal evolution of the oligomer products visualized by SIM clearly shows that the increased catalytic reaction rate results from the promotion of the accessibility to the zeolite crystals. We expect this work shed some light on the mechanistic insight into of the coupled surface mass transfer and reaction in zeolite catalysis.

Declaration of Competing Interest

The authors declare that they have no known competing financial interests or personal relationships that could have appeared to influence the work reported in this paper.

Acknowledgments

This work is supported by the National Natural Science Foundation of China (Grant No.91834302) and Innovation program of science and research from Dalian Institute of Chemical Physics (DICP I201938). The authors thank Dr. Linying Wang and Wenguang Yu in Dalian Institute of Chemical Physics, Chinese Academy of Sciences for the help with synthesis of ZSM-5 zeolites and IGA measurements.

Appendix A. Supplementary data

Supplementary data to this article can be found online at https://doi.org/10.1016/j.cej.2021.132760.

References

[1] C. Li, C. Yang, H. Shan, Maximizing propylene yield by two-stage riser catalytic cracking of heavy oil, Ind. Eng. Chem. Res. 46 (2007) 4914–4920, https://doi.org/10.1021/ie061420l.
[2] U. Olsbye, S. Svelle, M. Bjørgen, P. Beato, T.V.W. Janssens, F. Joensen, S. Bordiga, K.P. Lillerud, Conversion of methanol to hydrocarbons: how zeolite cavity and pore size controls product selectivity, Angew. Chem. Int. Ed. 51 (2012) 5810–5831, https://doi.org/10.1002/anie.201103657.
[3] H. Gies, B. Marler, C. Fyfe, G. Kokotailo, Y. Feng, D.E. Cox, The combination of synchrotron powder diffraction and high-resolution solid-state nmr experiments, J. Phys. Chem. Solids 52 (1991) 1235–1241, https://doi.org/10.1016/0022-3697(91)90198-9.
[4] B. Smit, T.L.M. Maesen, Towards a molecular understanding of shape selectivity, Nature 451 (2008) 671–678, https://doi.org/10.1038/nature06552.
[5] Z. Guo, X. Li, S. Hu, G. Ye, X. Zhou, M.-O. Coppens, Understanding the role of internal diffusion barriers in pt/beta zeolite catalyzed isomerization of n-heptane, Angew. Chem. Int. Ed. 59 (2020) 1548–1551, https://doi.org/10.1002/anie.201913660.
[6] G. Ye, Y. Sun, Z. Guo, K. Zhu, H. Liu, X. Zhou, M.-O. Coppens, Effects of zeolite particle size and internal grain boundaries on Pt/Beta catalyzed isomerization of n-pentane, J. Catal. 360 (2018) 152–159, https://doi.org/10.1016/j.jcat.2018.01.033.
[7] J. Kärger, D.M. Ruthven, Diffusion in nanoporous materials: fundamental principles, insights and challenges, New J. Chem. 40 (2016) 4027–4048, https://doi.org/10.1039/C5NJ02836A.
[8] J. Kärger, In-depth study of surface resistances in nanoporous materials by microscopic diffusion measurement, Micropor. Mesopor. Mater. 189 (2014) 126–135, https://doi.org/10.1016/j.micromeso.2013.11.023.
[9] S. Reitmeier, O. Gobin, A. Jentys, J. Lercher, Enhancement of sorption processes in the zeolite H-ZSM5 by postsynthetic surface modification, Angew. Chem. Int. Ed. 48 (2009) 533–538, https://doi.org/10.1002/anie.200803869.
[10] F. Hibbe, C. Chmelik, L. Heinke, S. Pramanik, J. Li, D.M. Ruthven, D. Tzoulaki, J. Kärger, The nature of surface barriers on nanoporous solids explored by microimaging of transient guest distributions, J. Am. Chem. Soc. 133 (2011) 2804–2807, https://doi.org/10.1021/ja108625z.
[11] G. Sastre, J. Kärger, D.M. Ruthven, Diffusion path reversibility confirms symmetry of surface barriers, J. Phys. Chem. C 123 (2019) 19596–19601, https://doi.org/10.1021/acs.jpcc.9b04528.
[12] L. Karwacki, H. vanderBij, J. Kornatowski, P. Cubillas, M. Drury, D.A.M. deWinter, M. Anderson, B. Weckhuysen, Unified internal architecture and surface barriers for molecular diffusion of microporous crystalline aluminophosphates, Angew. Chem. Int. Ed. 49 (2010) 6790–6794, https://doi.org/10.1002/anie.201003273.
[13] L. Karwacki, M.H.F. Kox, D.A. Matthijs de Winter, M.R. Drury, J.D. Meeldijk, E. Stavitski, W. Schmidt, M. Mertens, P. Cubillas, N. John, A. Chan, N. Kahn, S. R. Bare, M. Anderson, J. Kornatowski, B.M. Weckhuysen, Morphology-dependent zeolite intergrowth structures leading to distinct internal and outer-surface molecular diffusion barriers, Nat. Mater. 8 (2009) 959–965, https://doi.org/10.1038/nmat2530.
[14] G. Sastre, J. Kärger, D.M. Ruthven, Molecular dynamics study of diffusion and surface permeation of benzene in silicalite, J. Phys. Chem. C 122 (2018) 7217–7225, https://doi.org/10.1021/acs.jpcc.8b00520.
[15] M.R. Bonilla, T. Titze, F. Schmidt, D. Mehlhorn, C. Chmelik, R. Valiullin, S. K. Bhatia, S. Kaskel, R. Ryoo, J. Karger, Diffusion study by ir micro-imaging of molecular uptake and release on mesoporous zeolites of structure type CHA and LTA, Materials 6 (2013) 2662–2688, https://doi.org/10.3390/ma6072662.
[16] J. Kärger, T. Binder, C. Chmelik, F. Hibbe, H. Krautscheid, R. Krishna, J. Weitkamp, Microimaging of transient guest profiles to monitor mass transfer in nanoporous materials, Nat. Mater. 13 (2014) 333–343, https://doi.org/10.1038/nmat3917.
[17] D. Tzoulaki, L. Heinke, W. Schmidt, U. Wilczok, J. Karger, Exploring crystal morphology of nanoporous hosts from time-dependent guest profiles, Angew. Chem. Int. Ed. 47 (2008) 3954–3957, https://doi.org/10.1002/anie.200705597.
[18] J.C.S. Remi, A. Lauerer, C. Chmelik, I. Vandendael, H. Terryn, G.V. Baron, J.F. M. Denayer, J. Kärger, The role of crystal diversity in understanding mass transfer in nanoporous materials, Nat. Mater. 15 (2016) 401–406, https://doi.org/10.1038/nmat4510.
[19] S.M. Rao, E. Saraçi, R. Gläser, M.-O. Coppens, Surface barriers as dominant mechanism to transport limitations in hierarchically structured catalysts – Application to the zeolite-catalyzed alkylation of benzene with ethylene, Chem. Eng. J. 329 (2017) 45–55, https://doi.org/10.1016/j.cej.2017.04.015.
[20] S. Peng, M. Gao, H. Li, M. Yang, M. Ye, Z. Liu, Control of surface barriers in mass transfer to modulate methanol-to-olefins reaction over sapo-34 zeolites, Angew. Chem. Int. Ed. 59 (2020) 21945–21948, https://doi.org/10.1002/anie.202009230.
[21] S. Hu, J. Liu, G. Ye, X. Zhou, M.-O. Coppens, W. Yuan, Effect of external surface diffusion barriers on platinum/beta-catalyzed isomerization of n-pentane, Angew. Chem. Int. Ed. 60 (2021) 14394–14398, https://doi.org/10.1002/anie.202104859.
[22] M.J. Roeffaers, B. Sels, H. Uji-i, B. Blanpain, P. L'hoëst, P. Jacobs, F. DeSchryver, J. Hofkens, D. DeVos, Space- and time-resolved visualization of acid catalysis in ZSM-5 crystals by fluorescence microscopy, Angew. Chem. Int. Ed. 46 (2007) 1706–1709, https://doi.org/10.1002/anie.200604336.
[23] M.J. Roeffaers, G. De Cremer, J. Libeert, R. Ameloot, P. Dedecker, A.-J. Bons, M. Buckins, J.A. Martens, B.F. Sels, D.E. De Vos, J. Hofkens, Super-resolution reactivity mapping of nanostructured catalyst particles, Angew. Chem. Int. Ed. 48 (2009) 9285–9289, https://doi.org/10.1002/anie.200904944.
[24] Z. Ristanović, J.P. Hofmann, G. De Cremer, A.V. Kubarev, M. Rohnke, F. Meirer, J. Hofkens, M.B.J. Roeffaers, B.M. Weckhuysen, Quantitative 3d fluorescence imaging of single catalytic turnovers reveals spatiotemporal gradients in reactivity of zeolite h-zsm-5 crystals upon steaming, J. Am. Chem. Soc. 137 (2015) 6559–6568, https://doi.org/10.1021/jacs.5b01698.
[25] S. Sang, F. Chang, Z. Liu, C. He, Y. He, L. Xu, Difference of ZSM-5 zeolites synthesized with various templates, Catal. Today 93–95 (2004) 729–734, https://doi.org/10.1016/j.cattod.2004.06.091.
[26] M. Gao, H. Li, M. Yang, S. Gao, P. Wu, P. Tian, S. Xu, M. Ye, Z. Liu, Direct quantification of surface barriers for mass transfer in nanoporous crystalline materials, Commun. Chem. 2 (2019) 43, https://doi.org/10.1038/s42004-019-0144-1.
[27] J. Wloch, Effect of surface etching of ZSM-5 zeolite crystals on the rate of n-hexane sorption, Micropor. Mesopor. Mater. 62 (2003) 81–86, https://doi.org/10.1016/S1387-1811(03)00395-0.
[28] G. Ye, Z. Guo, Y. Sun, K. Zhu, H. Liu, X. Zhou, M.-O. Coppens, Probing the nature of surface barriers on zsm-5 by surface modification, Chem. Ing. Tech. 89 (2017) 1333–1342, https://doi.org/10.1002/cite.201700081.
[29] L. Karwacki, E. Stavitski, M.F. Kox, J. Kornatowski, B. Weckhuysen, Intergrowth structure of zeolite crystals as determined by optical and fluorescence microscopy of the template-removal process, Angew. Chem. Int. Ed. 46 (2007) 7228–7231, https://doi.org/10.1002/anie.200702012.
[30] Z. Diao, L. Wang, X. Zhang, G. Liu, Catalytic cracking of supercritical n -dodecane over meso-HZSM-5@Al-MCM-41 zeolites, Chem. Eng. Sci. 135 (2015) 452–460, https://doi.org/10.1016/j.ces.2014.12.048.
[31] Z. Diao, L. Cheng, W. Guo, X.u. Hou, P. Zheng, Q. Zhou, Fabrication and catalytic performance of meso-ZSM-5 zeolite encapsulated ferric oxide nanoparticles for phenol hydroxylation, Front. Chem. Sci. Eng. 15 (2021) 643–653, https://doi.org/10.1007/s11705-020-1972-3.
[32] G. Fleury, M.B.J. Roeffaers, Correlating acid site distribution and catalytic activity in dealuminated mordenite at the single-particle level, ACS Catal. 10 (2020) 14801–14809, https://doi.org/10.1021/acscatal.0c04144.